Biointerface Research in Applied Chemistry
Open-Access Journal (ISSN: 2069-5837)

Article
Volume 13, Issue 3, 2023, 214
https://doi.org/10.33263/BRIAC133.214

Effect of End Milling Process Parameters and Corrosion Behaviour of ZE41A Magnesium Alloy using Taguchi Based GRA

Rajender Kumar [1,2,*], Puneet Katyal [1], Kamal Kumar [3]

[1] Department of Mechanical Engineering, Guru Jambheshwar University of Science & Technology, Hisar
[2] Department of Basic Engineering, CCS Haryana Agricultural University, Hisar, India
[3] Department of Mechanical Engineering, Punjab Engineering College (Deemed to be University), Chandigarh
* Correspondence: rksingh1279@yahoo.com (R.K.);

Scopus Author ID 57220595867
Received: 10.03.2022; Accepted: 17.04.2022; Published: 5.06.2022

Abstract: The purpose of the study is to optimize the machining characteristics for milling ZE41A Mg alloy on a CNC milling by Taguchi-based Grey relational analysis (GRA) to achieve the maximum material removal rate (MRR), lowest corrosion rate (CR), and surface roughness (SR). After one week of immersion in simulated body fluid (SBF), weighing samples determined the corrosion rate. The process attributes, which include tool rotation cutting speed, feed rate, and depth of cut, are opted. The experiments were conducted using a Taguchi L_{16} orthogonal array (OA). Additionally, variance analysis (ANOVA) was used to determine the influence of process parameters on the responses. The study discusses the significance of machining process parameters concerning the degradation behavior of biomedical implant materials in a simulated body fluid (SBF). According to the current study, the most influential parameters in multi-objective optimization are the tool rotation cutting speed and feed rate. Thus, the results obtained with GRA of MRR: 492.25mm^3/min, SR: 0.3112µm, and CR: 6.386mm/year with the experimental confirmatory test were close to the expected values. ZE41A Mg alloy machined samples at optimum end-milling parameters enhanced performance in reduced surface roughness and low in-vitro corrosion rate for ZE41A Mg alloy.

Keywords: end milling; Mg alloy; machining characteristics; SBF; *In-vitro* corrosion; Taguchi method; Grey relational analysis.

1. Introduction

Many orthopedic and cardiovascular implants use inert metals due to their superior corrosion resistance and mechanical characteristics compared to the adjacent living tissues [1]. Traditionally, these metallic inserts are intended to retain in the body continuously until they are removed via intervention [2]. However, using stable, inert materials to provide temporary support can result in several complications, including stress shielding over the period, resulting in the implanted tissue weakening and the need for subsequent surgery to remove the implants. Thus, the utilization of biodegradable implants in the bodily location and gradual load transfer to recovering tissue until cell regeneration can be viable solutions for addressing the disadvantages of inert implants [3,4]. A possible biomaterial, magnesium (Mg), has developed due to its biocompatibility, mechanical strength, and ability to degrade in the environment. Mg is a harmless element found in nature, with an adult daily consumption of 240–420 mg/day

being the recommended amount. This amount is over fifty times greater than the acceptable quantity of iron and zinc; both of them are viable implant materials in addition to titanium. Furthermore, magnesium and its alloys have displayed impressive biocompatibility under physiological settings [5,6].

Magnesium exhibits desirable mechanical properties along with its biocompatibility for an implant. Additionally, the modulus of elasticity of magnesium is approximately 45 GPa, which is comparable to the bone, which eliminates the stress shielding problem [7]. Mg degrades rapidly in physiological circumstances, resulting in a loss of mechanical integrity resulting in implant failure. Another vital concern related to the fast deterioration of magnesium implants is excessive hydrogen (H_2) gas evolution. Accumulated gas bubbles can obstruct normal blood flow and cause tissue injury at implant sites [8,9]. Besides the fast uniform degradation caused by Mg's active nature, localized corrosion is yet another issue with Mg alloys. Localized corrosion is primarily caused by the growth of galvanic cells because of the potential difference between pure magnesium and its alloying components. Localized corrosion can result in the implant failing due to the degeneration of key sites. As a result, the factor of localized corrosion is a critical issue in alloy design. Therefore, this critical concern of deterioration must be addressed before the commercialization of magnesium implants. The ideal balance between mechanical strength, biodegradation rate, and biocompatibility has not yet been discovered [10,11].

Surface morphology such as surface roughness (SR), micro-cracks, and porosities all have an important role in the degradation rate of magnesium alloys that varies according to the processing method used. There has been conducted majority of research on alloying, even though there is a very scarcity of specialized literature on the machining of magnesium alloys [12,13]. Mg-alloys' low density facilitates better machining with the least power requirements, long tool life, and superior surface integrity [14]. Therefore, traditional machining operations such as grinding, drilling, milling, and turning must be emphasized for the fabrication of magnesium alloy bone implants. Typically, this is accomplished by material removal in the form of chips. The size and shape of the chip removal, the rate of material removed, and the good surface quality are all closely correlated to the cutting kinematic interaction with the workpiece [15]. Dimensional precision, mechanical piece performance, and cost of production are all affected by surface roughness [3]. G. Okkaya [16] observed that the optimal cutting speed for achieving the lowest roughness seems to be up to 200m/min with feed rate (FR). According to Santhanakrishnan *et al*. [17], the lowest value of SR (Ra) occurs at a higher speed and low feed rate. Al Hazza *et al*. [18] also identified the ideal surface roughness with a low feed rate and a high cutting speed. Increased FR results in an increased SR, lowering the quality of the surface finish [19].

Dry milling magnesium alloys is a cost-effective and environmentally friendly process that is widely utilized in industrial manufacturing as a high-performance cutting technique [20]. A rougher milled surface is more prone to pitting corrosion [21]. For WEDM machining, the corrosion rate increases with increasing SR due to the high discharge energy [22,23]. To obtain a high-quality surface with minimal degradation is required to employ optimization techniques to determine the ideal machining parameters. Using the Taguchi design approach, the paper analyses the effect of machining parameters on the surface characteristics of magnesium alloys [24,25]. The Taguchi method can systematically develop a procedural layout, analyze the significant effect of each investigational attribute using ANOVA, and finally determine the optimum parametric arrangement that results in the optimal milling situation. The S/N ratio

used by Taguchi can be used to reflect the mean (average) and variance (standard deviation) of results obtained [17].

Grey Relational Analytics (GRA) techniques are commonly used to improve conflict, discrete data issues, and multiple input methods. GRA has been used extensively to optimize different process attributes of manufacturing techniques such as drilling [26], end milling [27,28], dry turning [29,30], optimizing ECM process [31], TIG welding [32], and turning [33,34]. Dhiraj *et al*. [35] used Taguchi's method with different process variables by using GRA and TOPSIS implemented on AISI M2 steel. Many studies found that researchers used GRA with entropy measurement by allocating the entropy weight to each output to optimize the process parameters [36]. Machining has a substantial impact on magnesium alloy's surface properties that affect the degradation rate of the material. Therefore, tool rotation speed, FR, and depth of cut are selected as process parameters in this experiment.

In the present work, Taguchi's L_{16} orthogonal array (OA) was used to consider the milling process attributes for MRR, SR, and DR as response parameters. *GRA* approach was used to analyze multiple performance parameters. The primary objective is to determine the machining parameters that will result in the maximum MRR, minimize SR, and minimum DR during the end milling process. Additionally, bio-mineralization (apatite) and the morphology of machined surfaces were discussed concerning milling process parameters.

2. Materials and Methods

2.1. Materials.

The present study involves a sequence of machining tests on ZE41A Mg alloy using a CNC Milling (Hytech, model-MT250) machine. The milling operations are carried out in a dry environment. Milling was performed on workpiece samples of size 26 mm × 8 mm× 8 mm in triplicate. In the current investigation, an HSS end mill cutter of diameter 8 mm and four flutes was chosen as the cutting tool. The elemental composition of the material was determined by Wavelength Dispersive X-ray Fluorescence (WD-XRF) (Bruker, Germany), as given in Table 1. Mechanical, physical, and other Properties of material are given in Table 2. The structural characterization of milling samples was examined using a field emission scanning electron microscope (FESEM) (JEOL model JSM-7610F Plus). The material's microstructure and energy dispersive spectroscopy (EDS) analysis is shown in Figure 1(a, b). Fig. 2 illustrates the schematic process flow diagram used in this work on the ZE41A Mg alloy.

2.2. Experimental design.

The research is designed to determine the influence of process parameters on the performance of the finished surface, cutting speed, and degradation rate. The experimental matrix in this research is designed using the Taguchi design approach. The Taguchi method is a structured technique to experiment planning based on the design of orthogonal arrays (OA) and outcomes in significantly reducing the number of experiments while maintaining highly acceptable results. The Taguchi L_{16} (4^3) OA is used to control mainly process parameters: tool rotation cutting speed (TRS) in RPM, feed rate (mm/min), and depth of cut (mm), with their levels specified in Table 3 [37] that effected the surface roughness (Ra) of the machined substrate as taken by Kumar *et al*., 2022. According to Taguchi *OA* design L_{16}, experiments were conducted twice for each configuration, with the average data reported in Table 4.

TRS (RPM) has been computed in the current investigation by machining time over a sample length during the milling operation. Milled samples were analyzed using an SR tester (Mitutoyo-SJ410 model) to determine the average R_a value on the milled surface. After the immersion test, the stereo microscope (Carl-Zeiss, Stereo Discovery.V20) images show the apatite development on materials.

Table 1. Elemental composition of ZE41A Mg alloy [20].

Contents	Zn	Ce	Zr	Mn	La	Nd	Na	Al	Si	O	C	Pr	Cl	Mg
Wt%	4.2	0.58	0.54	0.02	0.25	0.15	0.26	0.02	0.06	0.58	5.23	0.04	0.03	Bal

Table 2. Mechanical, Physical, and other Properties of ZE41A Magnesium Alloy.

Mechanical Properties				Physical properties			Thermal Properties
Tensile strength, UTS (MPa)	Yield Tensile Strength, YTS (MPa)	Elongation, %	Micro-hardness (HV)	Young's modulus, GPa	Poisson's ratio	Density, g/cm^3	Thermal expansion coefficient (α) (µm/m°C)
218.38	90	4.63	65.1	44.12	0.35	1.84	15.1

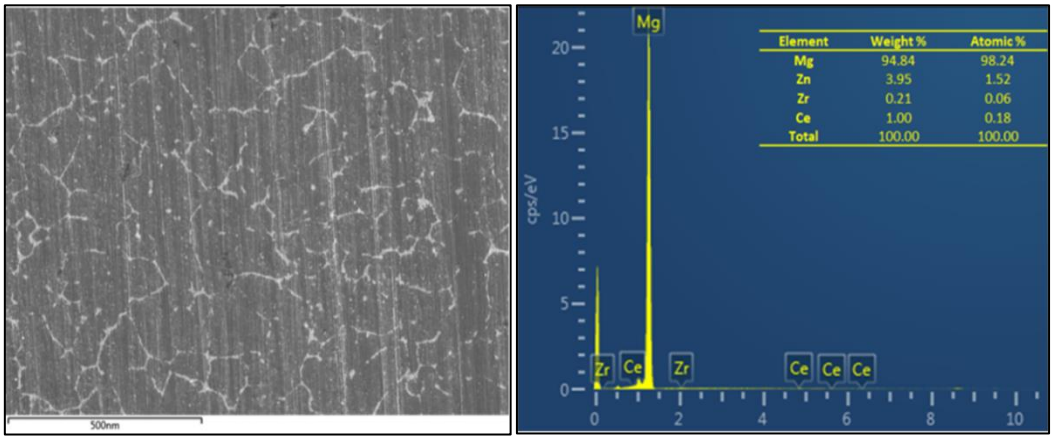

(a) (b)

Figure 1. (a) Microstructure and (b) EDS analyses of ZE41A Magnesium alloy.

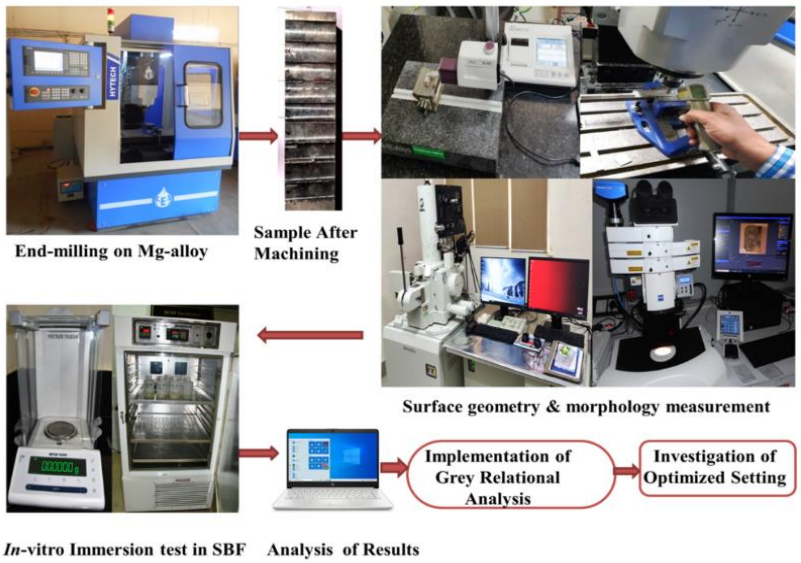

Figure 2. A schematic process flow diagram for the present experimental study on ZE41A Mg alloy.

2.3. In vitro immersion study.

The corrosion rate (mm/year) or degradation rate was determined by weighing (g) ZE41A samples after immersion for seven days in SBF held in BOD (Bio-Oxygen Demand)

incubator with 95% air and 5% CO_2 at 37±1^{0}C according to ASTM G31-72. SBF was prepared [38] to have the same pH as blood (7.40 ± 0.05) and ionic strength similar to those of human plasma [39]. For this test, the SBF volume of 0.20 ml/mm^2 was used for the material surface [40].

Magnesium alloys experience the most corrosion or deterioration in the first 7 days of exposure to SBF [22]; after that, the protective film thickens and decreases the rate of degradation. Thus, the degradation rate was considered through the period of 7 days of immersion in body fluid.

Thus, in this instance, the degradation rate was considered over the first 7 days of immersion in the fluid to ascertain the highest rate of degradation following milling under various parametric conditions. To remove corrosion products, magnesium alloy samples were washed with chromic acid and DI water after seven days, followed by an hour of oven drying at 60°C. The degradation in the form of corrosion rate was considered in mm/year using the weight loss equation (1) [6].

$$\text{Corrosion Rate (CR)} = \frac{K \times W}{A \times T \times \rho} \qquad \ldots\ldots\ldots (1)$$

Where W = weight loss (in grams), K = constant (8.76×10^4mm/year), A= area (cm^2), T =time of contact (hours), ρ=density of ZE41A (1.84 g/cm^3).

The apatite formation and modified surfaces after immersion and degradation were observed by a Carl-Zeiss stereo microscope.

Table 3. The process variables and their levels of machining of ZE41A Mg alloy.

Process Parameters	Symbol	Levels			
		1	2	3	4
Tool Rotation Cutting Speed (RPM)	TRS	1200	1700	2200	2700
Feed Rate (mm/min)	FR	25	50	75	100
Depth of Cut (mm)	DoC	0.5	0.75	1.0	1.25

Table 4. Experimental design using L_{16} OA and the responses.

Exp. No	Process parameters			Response parameters		
	TRS (RPM)	FR (mm/min)	DoC (mm)	MRR (mm^3/ min)	SR (R_a) (µm)	DR (mm/year)
1	1200	25	0.5	161.022	0.374	7.15
2	1200	50	0.75	485.902	0.452	7.81
3	1200	75	1	1008.634	0.566	8.05
4	1200	100	1.25	1702.565	0.679	8.63
5	1700	25	0.75	253.476	0.361	6.65
6	1700	50	0.5	355.115	0.379	7.29
7	1700	75	1.25	1236.260	0.416	7.92
8	1700	100	1	1337.825	0.478	7.94
9	2200	25	1	349.869	0.34	6.649
10	2200	50	1.25	864.136	0.386	7.48
11	2200	75	0.5	577.082	0.337	6.70
12	2200	100	0.75	1115.676	0.449	7.88
13	2700	25	1.25	445.512	0.306	6.287
14	2700	50	1	748.084	0.371	6.85
15	2700	75	0.75	857.699	0.392	7.41
16	2700	100	0.5	835.263	0.419	7.55

3. Results and Discussion

3.1. Analysis of process attributes on response parameter: Material Removal Rate (MRR).

The machinability of Mg-alloy is defined by the maximum MRR that may be induced during machining, which is the desired process parameter to be optimized. Maintaining a high MRR while controlling tool wear and limiting energy used by volume of chip removed are the

primary goals in the metal removal procedure. Figure 3 depicts the effect of change in process parameters on MRR. Table 4 summarises the investigational results for process attributes in the form of MRR, SR, and DR. As can be seen, each of the three factors had a noticeable effect on the MRR value during the milling of material. The effect of FR and DoC is more significant than that of TRS, as already confirmed by Sunil *et al*. [41], and can be seen in response Table 5. MRR reduces consistently between 1200 and 2700 rpm as cutting forces rise and hardness increases, influenced by a range of variables like cutting temperature, strain rate, etc. MRR consistently increases as FR and DoC values rise across all four stages. With FR and DoC, cutting force per unit area gradually increases with force amplitude, increasing material removal. Additionally, as the depth of the cut rises, the contact area expands, resulting in a greater MRR. In Figure 3, the feed rate exhibits the most variance, making it the most significant variable, followed by the DoC.

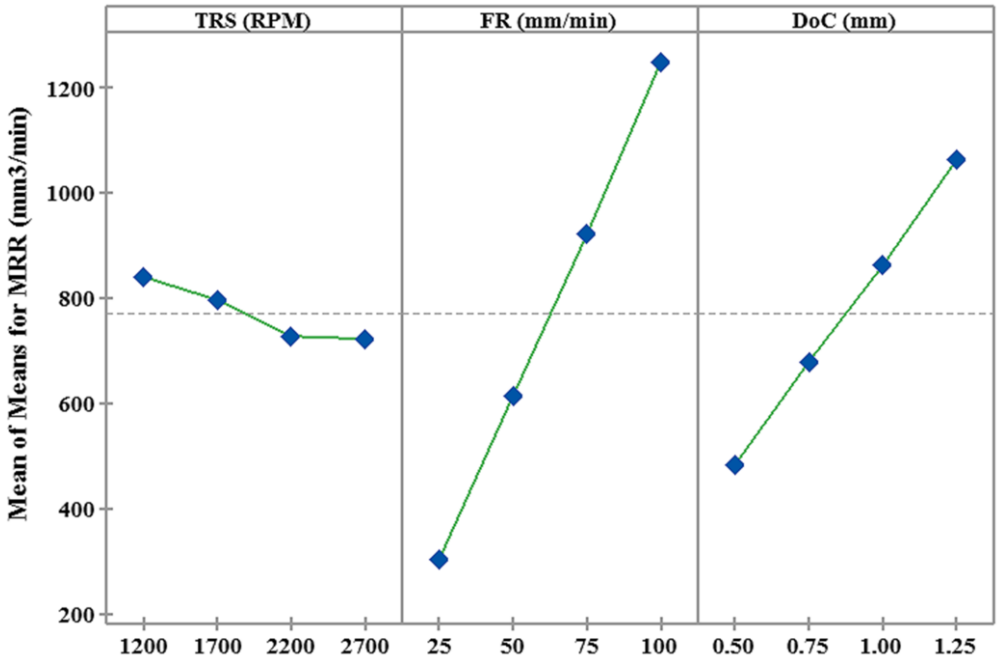

Figure 3. Effect of change in process parameters on MRR.

Table 5. Response Table for Means for MRR.

Level	TRS (RPM)	FR (mm/min)	DoC (mm)
1	839.5	302.5	482.1
2	795.7	613.3	678.2
3	726.7	919.9	861.1
4	721.6	1247.8	1062.1
Delta	117.9	945.4	580.0
Rank	3	1	2

To assess the influence of process parameters, variance analysis (ANOVA) with a 5% significance level on the output was considered. All process variables significantly influence MRR, as declared in Table 6. The most significant process variables for MRR are FR (74.11% contribution) and DoC (25.01% contribution). The maximum MRR is predicted at the characteristic settings TRS_1: 1200RPM; FR_4: 100mm/min; DoC_4: 1.25mm, with an anticipated S/N ratio of 64.3982 and a mean of 1607.72 obtained from the Taguchi analysis for single response optimization.

Table 6. Analysis of Variance for MRR.

Parameters	DF	Seq SS	Adj MS	F-Value	P-Value	Contribution
TRS (RPM)	3	0.05095	0.01698	18.93	0.002	0.79%
FR (mm/min)	3	4.75126	1.58375	1765.24	0.000	74.11%
DoC (mm)	3	1.60366	0.53455	595.81	0.000	25.01%
Error	6	0.00538	0.00090			0.08%
Total	15	6.41126				100.00%

3.2. Effect of process variables on Surface Roughness (SR).

The surface integrity of magnesium based products can use to forecast their performance because surface imperfections are a major source of corrosion [42]. By altering the roughness of the implant surface, cell and tissue response can be improved by enhancing the implant area close to the bone and therefore boosting cell adhesion to the bone. Various parameters, including roughness, texture, and direction of imperfections, have been used to classify implant surfaces. There are three levels of roughness for implant surfaces: slightly rough (0.5-1m), intermediately rough (1-1.5m), and severe rough (2-3m) surfaces. Concave and convex textures can be seen on the surface of implants, which can be categorized as either additive or subtractive treatments, such as hydroxyapatite (HA) coating or titanium plasma spraying. The abnormalities on the implant's surface can also be categorized: A isotropic surface is one that has the same topography regardless of the measurement direction. Directionality and variation in roughness are two characteristics of anisotropic surfaces [43]. As many studies show, the cutting variables have a significant effect on the SR [44]. From 1200 rpm to 2700 rpm, the SR declines in proportion to the TRS (see Fig. 4). TRS increases result in more heat being generated at the work surface, which softens the material and reduces the cutting force needed to cut the material. So, as a result, with increasing TRS, surface roughness reduces. In addition, fast cutting speeds decreased built-up edges and scaling effects, which resulted in a decline in the SR [45].

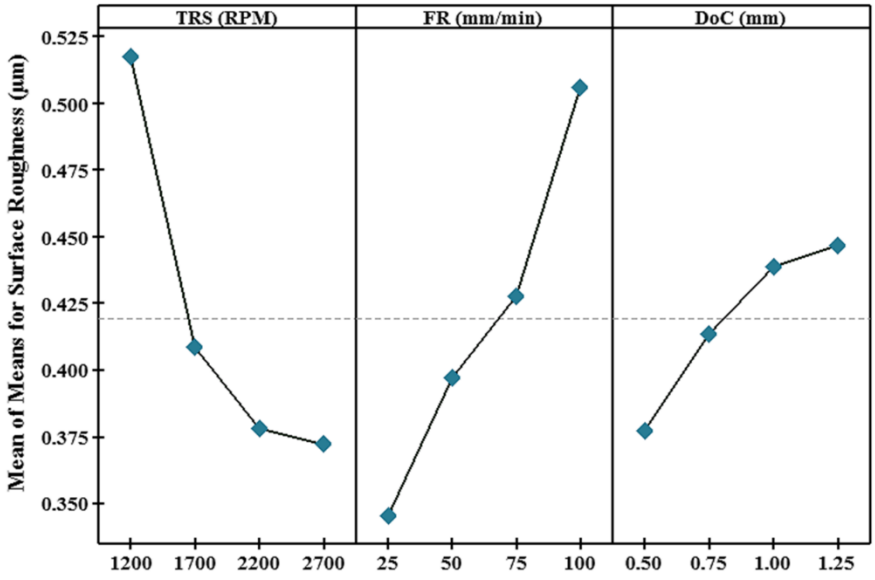

Figure 4. Effect of change in process parameters on SR.

As shown in Fig 4, SR significantly enhances with FR and DoC. The material rate removed due to shear and cutting forces has increased, as discussed in an earlier section, due to the increase of FR and DoC. Higher built-up edges can be seen afterward with high DoC, which increases roughness [46]. To achieve a smoother finish, the higher TRS (2700 RPM)

and lower FR and DoC (0.5mm) values decreased SR. Chips attach to the tool face because of the cutting tool friction, affecting tool life and surface morphology [47]. The surface topography of machined surfaces captured by SEM in the experiments is shown in Figs. 5 (a) and (b). Feed marks, plowing grooves, micro-pits, metal debris, cracks, and other surface imperfections can be seen on the Mg sample's machined surface. Work hardening occurs due to increased FR and DoC, which increase cutting force and deformation. SEM in Fig 5(a) shows that the surface noticed the plowing and perturbances generated while milling samples.

Table 7. ANOVA for SR.

Parameters	DF	Seq SS	Adj MS	F-Value	P-Value	Contribution
TRS (RPM)	3	1.2081	0.40269	14.72	0.004	38.90%
FR (mm/min)	3	1.5340	0.51135	18.69	0.002	49.40%
DoC (mm)	3	0.1992	0.06639	2.43	0.164	6.41%
Error	6	0.1641	0.02735			5.29%
Total	15	3.1054				100.00%

TRS and FR are extremely influencing variables having a P-Value ≤ 0.05 impacting the SR, accounting for 38.90% and 49.40% of its total effect on the SR, respectively (Table 7). Figure 4 shows that the least SR attained relates to the settings of TRS_4:2700RPM; FR_1:25mm/min; DoC_1:0.5mm; and predicted S/N ratio of 10.9421 and Mean of 0.256375 determined by the Taguchi techniques for SR.

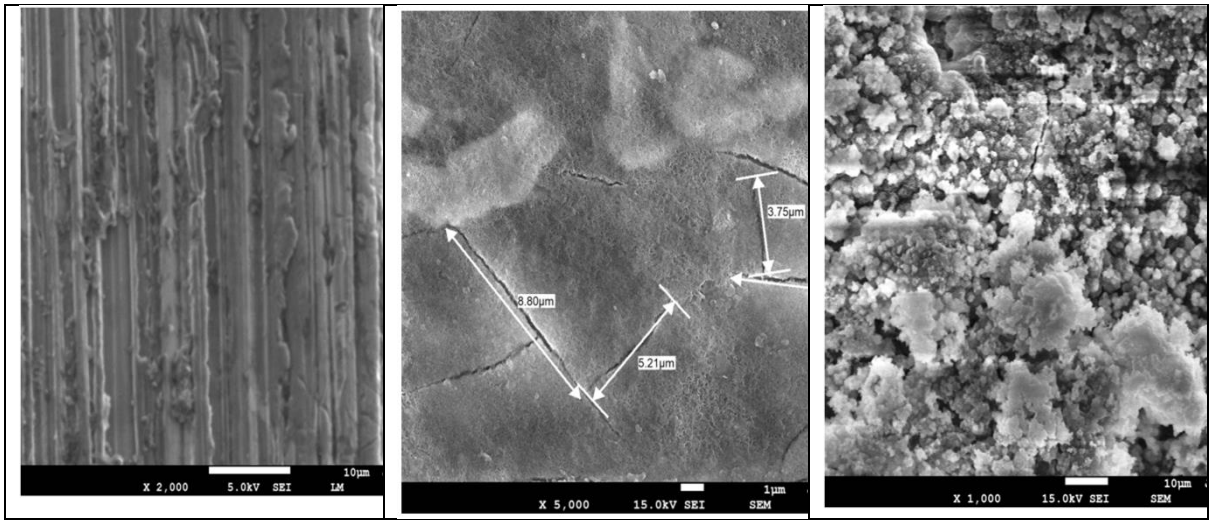

Figure 5. SEM images of the ZE41A Mg samples (a) Milled surface (b) micro-cracks observed on the machined surface (c) apatite formation on the machined surface of Mg alloy.

3.3. Effect of process variables on Degradation Rate (DR).

After immersing ZE41A samples in SBF for seven days, the corrosion in the form of DR (mm/year) has been computed by equation (1). The degradation rate (DR) is proportionate to the weight loss rate (mg/cm^2/day) that relies heavily on the material's surface properties through which the SBF accesses and promotes corrosion. Weight loss is detected due to released ions in the SBF solution via anodic dissolution and depends on the immersion period. When Mg-alloy is submerged in SBF, it has been observed that the metal ions are released at a quicker rate during the first few days of exposure and subsequently decrease as the immersion period increases. As a result, seven days of immersion were chosen for this investigation to obtain a consensus estimate of the corrosion rate. Dry machining operations resulted in a drop in DR as surface integrity improves due to increasing TRS and decreased cutting forces because of the working sample's thermal softening. Figure 6 illustrates the effect of change in process

parameters on DR of ZE41A Mg alloy. DR gradually increases with a feed rate (FR) of 25 to 100 mm/min. By increasing the FR, the cutting tool's travel speed over the working sample is increased, reducing the available time for heat to be delivered to the work material. As a result, most of the heat created is passed through the metal chips rather than the work material. Additionally, extreme plowing causes an increase in surface roughness and burr growth, which increases DR. Increased DoC makes the contact area increase between the metal chips and tool-tip, which results in increased temperature generation at the tool-tip, which results in the formation of built-up edges. Due to the degradation of the surface morphology caused by the built-up edge, DR increases as the DoC enhances to 1.25 mm.

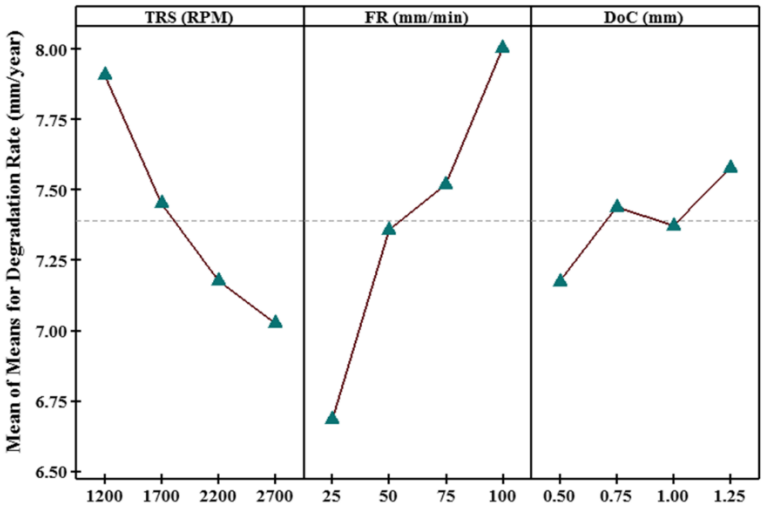

Figure 6. Effect of change in process parameters on DR.

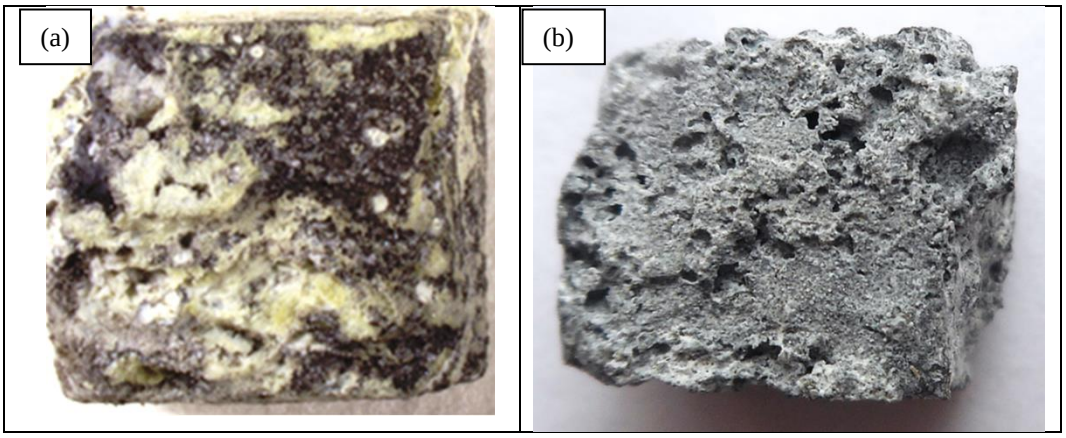

Figure 7. Surface morphology observed by stereo microscope (a) before and (b) after removal of apatite from the samples after immersion in SBF.

SEM images show micro-cracks on the machined substrate due to residual stress generation, as shown in Figure 5(b) by SEM images. Micro-cracks are effective attractors for bodily fluid (SBF) to penetrate beneath the substrate; they may attract the corrosion site to become more exposed. Following seven days of immersion in SBF, Figs. 5 (c) and 7 (a) indicate the apatite formation (bio-mineralization) by SEM and stereo microscope, and Fig 7 (b) shows corroded states after removing apatite corresponding to samples after immersion in SBF. Larger crack densities and wider cracks indicate a faster degradation rate.

Fig 8 of FESEM and EDS analysis determined the machined samples having apatite deposition with majorly constituent elements of *Ca, Mn, Na, P*, and *Mg* [48], and the presence of element O reflects the oxidation that takes place during machining and after that in immersion.

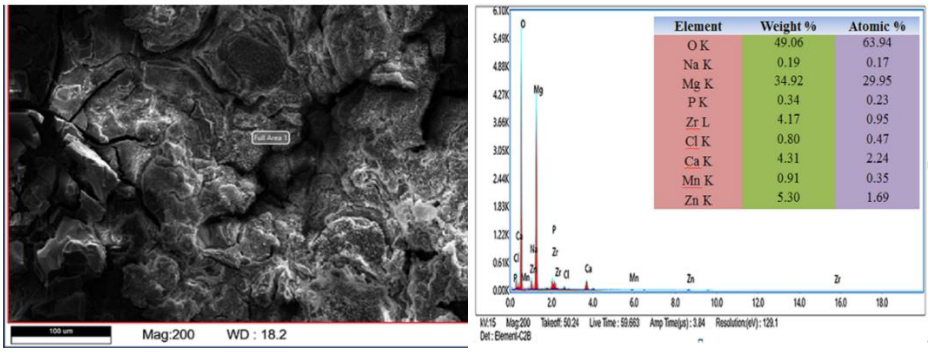

Figure 8. (a) FESEM and (b) EDS analysis of apatite formed on the machined sample with mineralization elements.

As depicted in Fig. 7 (b), removing corrosion products reveal micro-porosity and localized degradation on the substrate surface, and degraded geometry clearly distinguishes weight loss criteria. Many studies reported the alloys' deterioration mechanisms in physiological environments and highlighted the difference between the rate of bone repair and alloy degradation due to fast corrosion, which reflects the challenge in biomedical applications of Mg alloys [49].

Table 8. Analysis of Variance for DR.

Parameters	DF	Seq SS	Adj MS	F-Value	P-Value	Contribution
TRS (RPM)	3	2.2301	0.74337	16.02	0.003	31.88%
FR (mm/min)	3	3.7871	1.26236	27.21	0.001	54.14%
DoC (mm)	3	0.6999	0.23331	5.03	0.045	10.01%
Error	6	0.2784	0.04640			3.98%
Total	15	6.9955				100.00%

ANOVA is used to compute the DR. TRS and FR are both significant, as indicated in Table 8, followed by TRS, as illustrated in Figure 6. TRS_4:2700RPM; FR_1:25mm/min; DoC_1:0.5mm is the projected parametric setting for minimum DR and expected S/N ratio -15.8229 and Mean 6.10146 using the Taguchi approach for DR.

3.4. Grey relational analysis: multiple response optimization technique.

3.4.1. Taguchi-based Grey relation optimization.

Increased MRR, decreased SR, and DR are recommended requirements for optimizing machining process parameters. GRA is used to optimize multiple influencing factors with multiple feature characteristics simultaneously. The grey relational grade (GRG) establishes the quality condition on a 'larger is better' basis, prioritizing the best acceptable response characteristics [50]. The process flow adopted for GRA is given in Fig. 9.

All experimental results are normalized to a value between 0 and 1. Because data patterns were compared using a variety of levels and units, pre-processing is extremely beneficial in GRA. Figure 10 illustrates the workflow for determining GRG. The quality requirements for output characteristics in this study include maximization of MRR, and thus mean values for MRR were normalized using Eq (2). The present investigation's quality requirements for performance parameters include the maximization of MRR, and hence mean values for MRR were normalized using Eq (2). For surface roughness and corrosion rate, the lower, the better response adopted and the normalization done as perusing Eq (3).

A. Data Pre-processing and Normalizing mean data of Response Parameters:

a) Larger the better characteristics

$$Y_i(k) = \frac{\{X_i(k) - \min X_i(k)\}}{\{\max X_i(k) - \min X_i(k)\}} \ldots\ldots (2)$$

b) Smaller the better Characteristics

$$Y_i(k) = \frac{\{\max X_i(k) - X_i(k)\}}{\{\max X_i(k) - \min X_i(k)\}} \ldots\ldots (3)$$

Where; $Y_i\ (k)$ is a grey relational generation of normalized values; $X_i\ (k)$ is measured experimental mean values,

max Xi (k) = highestvalue for the k^{th} term

min Xi (k) = lowest value for k^{th} term (k = 1,2,3; response characteristics)

B. Calculation of Deviation Sequence and Grey relational coefficient (F_i):

$$F_i(k) = \frac{(\Delta_{min} + \Psi\Delta_{max})}{(\Delta_{Oi}(k) + \Psi\Delta_{max})} \ldots\ldots (4)$$

Where, the deviation sequence $[\Delta_{0i}(k)] = |Y_o\ (k) - Y_i\ (k)|$, Ψ= characteristic coefficient, which ranges from 0 ≤ Ψ ≤ 1 and is selected as 0.5 in the present work. Δ_{min}= minimum response for Δ_{0i} and $\Delta_{max}$is the maximum responsefor the Δ_{0i}.

C. Computation of Grey Relational Grade (χ):

$$\chi_i = 1/n\{\sum_{k=1}^{n} w_k\, F_i(k)\} \ldots\ldots (5)$$

Where n is the number of performance parameters and w = weight of the k^{th} performance attribute

$$\sum_{i=1}^{n} w_i = 1 \ldots\ldots\ldots (6)$$

D. Estimation of Grey relational grade (GRG) at optimal settings and Confirmation Experiment:

$$\chi_{opt} = \chi_m + \sum_{i=1}^{q} (\chi i - \chi m) \ldots\ldots (7)$$

χ_{opt} = optimal grey relational grade (estimated); χ_m = total mean of *GRG*; χi = mean of the GRG at the optimal level, and q is the number of significant process parameters.

Figure 9. The process flow used in GRA for computing and analyzing GRG.

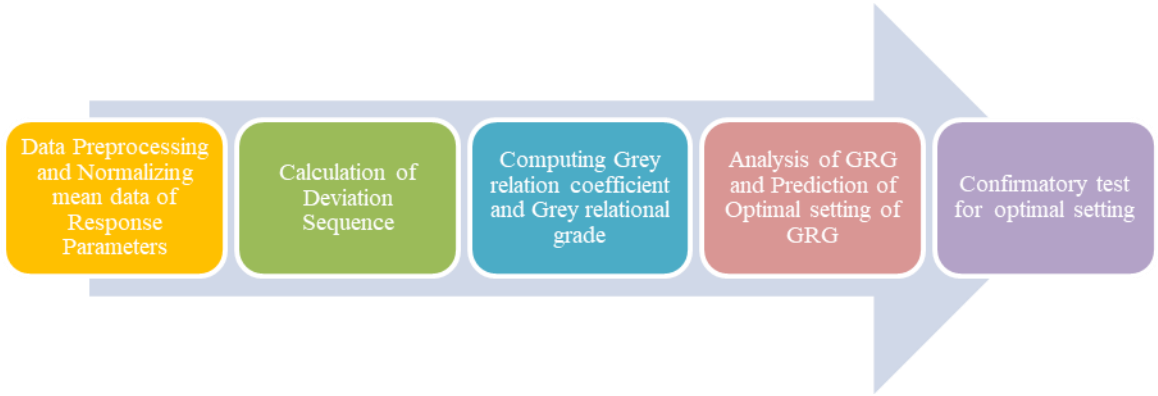

Figure 10. General steps of GRA technique.

Table 9. Pre-processing of data and determination of the grey relational grade (GRG).

Exp. No.	Normalization means response parameters			Deviation sequence			Grey relational coefficient (GRC)			GRG	Rank
	MRR	SR	DR	MRR	SR	DR	MRR	SR	DR		
1	0.00	0.818	0.633	1.00	0.18	0.37	0.333	0.733	0.577	0.558	8
2	0.21	0.609	0.351	0.79	0.39	0.65	0.388	0.561	0.435	0.465	15
3	0.55	0.303	0.246	0.45	0.70	0.75	0.526	0.418	0.399	0.444	16
4	1.00	0.000	0.000	0.00	1.00	1.00	1.000	0.333	0.333	0.533	11
5	0.06	0.853	0.845	0.94	0.15	0.16	0.347	0.772	0.763	0.642	4
6	0.13	0.804	0.570	0.87	0.20	0.43	0.364	0.719	0.537	0.549	10
7	0.70	0.705	0.303	0.30	0.29	0.70	0.623	0.629	0.418	0.553	9

Exp. No.	Normalization means response parameters			Deviation sequence			Grey relational coefficient (GRC)			GRG	Rank
	MRR	SR	DR	MRR	SR	DR	MRR	SR	DR		
8	0.76	0.539	0.295	0.24	0.46	0.70	0.679	0.520	0.415	0.531	12
9	0.12	0.909	0.845	0.88	0.09	0.15	0.363	0.846	0.764	0.672	3
10	0.46	0.786	0.492	0.54	0.21	0.51	0.479	0.700	0.496	0.562	6
11	0.27	0.917	0.825	0.73	0.08	0.17	0.406	0.857	0.741	0.681	2
12	0.62	0.617	0.317	0.38	0.38	0.68	0.568	0.566	0.423	0.516	14
13	0.18	1.000	1.000	0.82	0.00	0.00	0.380	1.000	1.000	0.814	**1**
14	0.38	0.826	0.760	0.62	0.17	0.24	0.447	0.742	0.676	0.630	5
15	0.45	0.769	0.521	0.55	0.23	0.48	0.477	0.684	0.511	0.561	7
16	0.44	0.697	0.458	0.56	0.30	0.54	0.471	0.623	0.480	0.527	13

In this case, GRG was determined by Eqn 5 by allocating the following weights to each characteristic: MRR: 30%, SR: 35%, and DR: 35%, with the consideration that each parameter desirability is mostly based on surface roughness and degradation. Experiment No 13 has the maximum value of GRG reflecting the optimum results; therefore, the optimal set of parametric values is determined. The computed GRC and GRG are declared in Table 9. The objective is to optimize MRR, SR, and DR with the optimal parameter combination concerning a larger GRG value.

ANOVA, a variance analysis using Minitab 19 version, has confirmed that process variables substantially affect the output at the 95% confidence level. The larger, the better criteria were used to evaluate the GRG values. Table 10 responds using GRG. ANOVA Table 11 illustrates the TRS (37.55%), FR (35.45%), and DoC (7.55%) contribution to the GRG computation. The maximum GRG is predicted at the characteristic settings TRS_4: 2700RPM; FR_1: 25mm/min; DoC_4: 1.25mm, with an anticipated S/N ratio of -2.25012 and a mean of 0.765443 obtained from the Taguchi analysis for single response optimization as shown in Fig. 11.

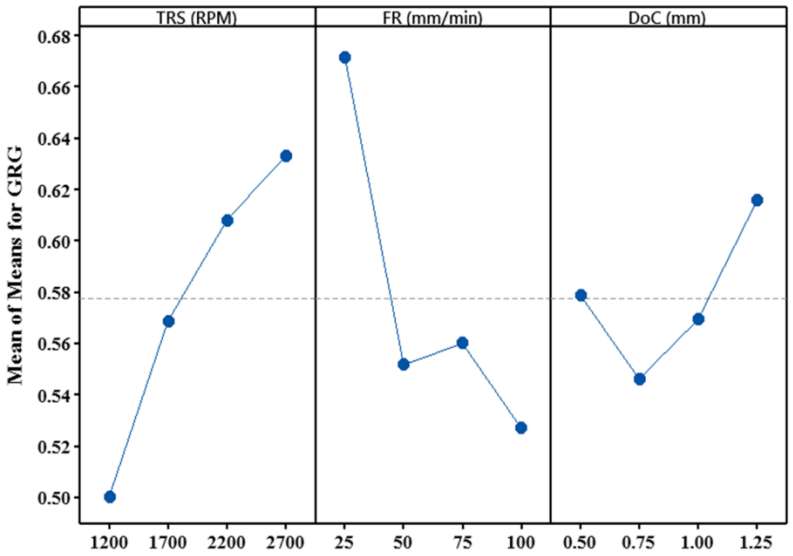

Figure 11. Effect of change in process parameters on GRG.

Table 10. Response Table for Means for Grey Relational Grade.

Level	TRS (RPM)	FR (mm/min)	DoC (mm)
1	0.5001	0.6715	0.5789
2	0.5686	0.5515	0.5461
3	0.6081	0.5600	0.5693
4	0.6332	0.5270	0.6157
Delta	0.1331	0.1446	0.0696
Rank	2	1	3

Table 11. ANOVA for Grey Relational Grade.

Parameters	DF	Seq SS	Adj MS	F-Value	P-Value	Contribution
TRS (RPM)	3	0.37338	0.12446	3.86	0.075	37.55%
FR (mm/min)	3	0.35251	0.11750	3.65	0.083	35.45%
DoC (mm)	3	0.07512	0.02504	0.78	0.548	7.55%
Error	6	0.19336	0.03223			19.45%
Total	15	0.99437				100.00%

3.4.2. Computing optimal value for GRG and a confirmatory test.

ANOVA, which reveals the most significant characteristics, can forecast GRG's optimum values. Three process attributes are considered in this case while establishing the optimal GRG value. It has been estimated by determining GRG at optimum settings using Equation 7, and the predicted GRG value is 0.7654.

χ_{opt} (estimated)=0.5775+(0.6332-0.5775)+(0.6715-0.5775)+(0.6157-0.5775)=0.7654

Table 12. Multi response optimization using GRA and confirmatory experimental results.

Method	Response	Optimal condition		% deviation ± (P-E) /P*100
		Predicted/expected optimal value (P)	Experimental value (E)	
		TRS_4-F_1-D_4	TRS_4-F_1-D_4	
GRA based Multi response optimization	*MRR* (mm^3/min)	544.46	492.25	-9.59%
	SR (µm)	0.3259	0.3112	4.51%
	DR (mm/Year)	6.5058	6.386	1.84%

Similarly for Material Removal Rate:

The entire mean MRRµ = 770.88 mm^3/min, so the estimated value of MRR is computed as

MRRp = (Tm_4+ Fm_1+ Dm_4) – (q-1) MRRµ (where q = number of process variables used)

= (721.639+302.47 +1062.12) – 2*770.88 = 544.46 mm^3/min

For Surface Roughness: SR_p =0.3259µm

For Degradation Rate: DR_p = 6.5058 mm/year

The GRG is anticipated based on the experiment results listed in Table 9, with process attributes established at each level. Table 12 describes the best-expected values and experiment results for multi-response optimization. Investigation No. 13 (Table 9) has the greatest GRG (0.814), exhibiting the optimal multiple performance characteristics using the process set of *TRS_4-FR_1-DoC_4*.

To authenticate the optimum outcome estimated through Taguchi based *GRA*, the experiments were conducted using the optimal combination of *TRS*-2700RPM; *FR*-25mm/min; *DoC*-1.25mm for *MRR*: 492.25 mm^3/min, SR: 0.3112µm, and DR: 6.386 mm/year as noticed in Table 12. The experimental results are close to the expected values.

4. Conclusions

The end-milling characteristics TRS, FR, and DoC were investigated experimentally for the ZE41A magnesium alloy. The experimental design was planned using Taguchi-based L_{16} OA, and the multi-objective optimization was performed using the grey relational analysis MRR, SR, and DR values were decreased due to increasing TRS. The FR has a greater effect on all three performance parameters. Since the cutting forces and volume of working sample sheared per unit time involved have grown with increasing FR and DoC; MRR, SR, and DR have risen substantially. It is noticed that the residual stresses are generated along the grain boundaries as the ZE41A surface compresses immediately after machining with chip removal. Thus, generated micro-cracks in Mg-alloy in SBF increase the degradation rate. In the present

experiment, the Taguchi technique found the optimal process parameters for each performance characteristic, and the results were as follows: TRS_1-1200RPM; FR_4-100mm/min; DoC_4-1.25mm for maximum MRR; TRS_4-2700RPM; FR_1-25mm/min; DoC_1-0.5mm for minimum SR and DR. However, Taguchi-based GRA recommended that the TRS_4-2700RPM; FR_1-25mm/min; DoC_4-1.25mm is the optimal combination for multi-objective optimization. The biomineralization (or corrosion rate) increases with increasing surface crack density, according to the Immersion investigations. Thus apatite elements such as Ca, Mg, P, and Na are the most common in mineralized products in developing apatite, according to EDS.

Further research can be considered the impact of surface properties with H_2 evolution rate and mechanical strength loss with ion release rate through Atomic absorption spectroscopy (AAS)/ Microwave plasma atomic emission spectroscopy (MP-AES) etc, for an extended period of immersion to determine the end milling procedure for making biodegradable magnesium alloy implants.

Funding

This research received no external funding.

Acknowledgments

The authors are grateful to the Biochemistry Laboratory, Department of Genetics and Plant Breeding, CCS Haryana Agricultural University, Hisar, India, for providing facilities to carry out this work.

Conflicts of Interest

The authors declare no conflict of interest.

References

1. Joung, Y.H. Development of implantable medical devices: from an engineering perspective. *International neurourology journal* **2013**, *17*, 98-106; https://doi.org/10.5213/inj.2013.17.3.98.
2. Han, H.S.; Loffredo, S.; Jun, I.; Edwards, J.; Kim, Y.C.; Seok, H.K.; Witte, F.; Mantovani, D.; Glyn-Jones, S. Current status and outlook on the clinical translation of biodegradable metals. *Materials Today* **2019**, *23*, 57-71; https://doi.org/10.1016/j.mattod.2018.05.018.
3. Tai, C.C.; Lo, H.L.; Liaw, C.K.; Huang, Y.M.; Huang, Y.H.; Yang, K.Y.; Huang, C.C.; Huang, S.I.; Shen, H.H.; Lin, T.H.; Lu, C.K. Biocompatibility and biological performance evaluation of additive-manufactured bioabsorbable iron-based porous suture anchor in a rabbit model. *International journal of molecular sciences* **2021**, *22*, https://doi.org/10.3390/ijms22147368.
4. Singh, V.; Katyal, P.; Kumar, K.; Kumar, R. Surface Integrity and Biological Response of Ti-Alloy Implants after Surface Modification. *Materials Today: Proceedings* **2021**, *56*, 2451-2468, https://doi.org/10.1016/j.matpr.2021.08.235.
5. Chen, Y.; Xu, Z.; Smith, C.; Sankar, J. Recent advances on the development of magnesium alloys for biodegradable implants. *Acta biomaterialia* **2014**, *10*, 4561-73, https://doi.org/10.1016/j.actbio.2014.07.005.
6. Abdel Gawad, M.; Usman, C.A.; Shunmugasamy, V.C.; Karaman, I.; Mansoor, B. Corrosion behavior of Mg-Zn-Zr-RE alloys under physiological environment–Impact on mechanical integrity and biocompatibility. *Journal of Magnesium and Alloys* **2021**, https://doi.org/10.1016/j.jma.2021.11.025.
7. Song, G. Control of biodegradation of biocompatable magnesium alloys. *Corrosion Science* **2007**, *49*, 1696-1701, https://doi.org/10.1016/j.corsci.2007.01.001.
8. Riaz, U.; Shabib, I.; Haider, W. The current trends of Mg alloys in biomedical applications—A review. *Journal of Biomedical Materials Research Part B: Applied Biomaterials* **2019**, *107*, 1970-1996, https://doi.org/10.1002/jbm.b.34290.
9. Kumar, S.; Katyal, P.; Chaudhary, R.N.; Singh, V. Assessment of factors influencing bio-corrosion of magnesium based alloy implants: A review. *Materials Today: Proceedings* **2022**, *56*, 2680-2689, https://doi.org/10.1016/j.matpr.2021.09.262.

10. Sharma, G.; Kumar, K.; Satsangi, P.S.; Sharma, N. Surface Modification of Biodegradable Mg-4Zn Alloy Using PMEDM: An Experimental Investigation, Optimization and Corrosion Analysis. *IRBM* **2021**, https://doi.org/10.1016/j.irbm.2021.02.003.
11. Yang, Y.; Xiong, X.; Chen, J.; Peng, X.; Chen, D.; Pan, F. Research advances in magnesium and magnesium alloys worldwide in 2020. *Journal of Magnesium and Alloys* **2021**, *9*, 705-747, https://doi.org/10.1016/j.jma.2021.04.001.
12. Uddin, M.S.; Rosman, H.; Hall, C.; Murphy, P. Enhancing the corrosion resistance of biodegradable Mg-based alloy by machining-induced surface integrity: influence of machining parameters on surface roughness and hardness. *The International Journal of Advanced Manufacturing Technology* **2017**, *90*, 2095-2108, https://doi.org/10.1007/s00170-016-9536-x.
13. Kumar, R.; Katyal, P. Effects of alloying elements on performance of biodegradable magnesium alloy. *Materials Today: Proceedings* **2022**, *56*, 2443-2450, https://doi.org/10.1016/j.matpr.2021.08.233.
14. Kumar, R.; Promila; Kumar, A.; Silla, S.; Sarova, A. Biocompatibility and degradation study of magnesium alloys: a review. *International Journal of Emerging Technologies and Innovative Research* **2017**, *4*, 526-536, http://doi.one/10.1729/Journal.29426.
15. Sheikh-Ahmad, J.Y. *Machining of polymer composites.* New York: Springer; **2009**; https://doi.org/10.1007/978-0-387-68619-6.
16. Gökkaya, H. The Effects of Machining Parameters on Cutting Forces, Surface Roughness, Built-Up Edge (BUE) and Built-Up Layer (BUL) During Machining AA2014 (T4) Alloy. *Strojniski Vestnik/Journal of Mechanical Engineering* **2010**, *56*, 584-593.
17. Santhanakrishnan, G.; Krishnamurthy, R.; Malhotra, S.K. Machinability characteristics of fibre reinforced plastics composites. *Journal of Mechanical Working Technology* **1988**, *17*, 195-204, https://doi.org/10.1016/0378-3804(88)90021-6.
18. Al Hazza, M.H.; Adesta, E.Y. Investigation of the effect of cutting speed on the Surface Roughness parameters in CNC End Milling using Artificial Neural Network. *IOP conference series: materials science and engineering* **2013**, *53*, https://doi.org/10.1088/1757-899X/53/1/012089.
19. Nurhaniza, M.; Ariffin, M.K.A.M.; Mustapha, F.; Baharudin, B.T.H.T. Analyzing the Effect of Machining Parameters Setting to the Surface Roughness during End Milling of CFRP-Aluminium Composite Laminates. *International Journal of Manufacturing Engineering* **2016**, *2016*, 1-9, https://doi.org/10.1155/2016/4680380.
20. Kumar, R.; Katyal, P.; Kumar, K.; Singh, V. Multiresponse optimization of end milling process parameters on ZE41A Mg alloy using Taguchi and TOPSIS approach. *Materials Today: Proceedings* **2022**, *56*, 2497-2504, https://doi.org/10.1016/j.matpr.2021.08.271.
21. Walter, R.; Kannan, M.B.; He, Y.; Sandham, A. Effect of surface roughness on the in vitro degradation behaviour of a biodegradable magnesium-based alloy. *Applied Surface Science* **2013**, *279*, 343-348, https://doi.org/10.1016/j.apsusc.2013.04.096.
22. Gill, R.S.; Kumar, K.; Batra, U. Surface Characteristics and Corrosion Behavior of Wire Electrical Discharge Machining Processed Mg-4Zn Alloy. *Journal of Materials Engineering and Performance* **2021**, *30*, 2955-2966, https://doi.org/10.1007/s11665-021-05525-6.
23. Singh, N.; Batra, U.; Kumar, K.; Mahapatro, A. Evaluation of corrosion resistance, mechanical integrity loss and biocompatibility of PCL/HA/TiO2 hybrid coated biodegradable ZM21 Mg alloy. *Journal of Magnesium and Alloys* **2021**, https://doi.org/10.1016/j.jma.2021.10.004.
24. Goyal, K.K.; Sharma, N.; Gupta, R.D.; Gupta, S.; Rani, D.; Kumar, D.; Sharma, V.S. Measurement of performance characteristics of WEDM while processing AZ31 Mg-alloy using Levy flight MOGWO for orthopedic application. *The International Journal of Advanced Manufacturing Technology* **2022**, *119*, 7175-7197, https://doi.org/10.1007/s00170-021-08358-8.
25. Selvakumar, G.; Ram Prakash, S.; Caleb Kovilpillai, E. Machining of ZE41 magnesium alloy in WEDM using taguchi approach. *Trends in Manufacturing and Engineering Management*. **2021**, 747-53, https://doi.org/10.1007/978-981-15-4745-4_66.
26. Tosun, N. Determination of optimum parameters for multi-performance characteristics in drilling by using grey relational analysis. *The International Journal of Advanced Manufacturing Technology* **2006**, *28*, 450-455, https://doi.org/10.1007/s00170-004-2386-y.
27. Rajeswari, B.; Amirthagadeswaran, K.S. Experimental investigation of machinability characteristics and multi-response optimization of end milling in aluminium composites using RSM based grey relational analysis. *Measurement* **2017**, *105*, 78-86, https://doi.org/10.1016/j.measurement.2017.04.014.
28. Shihab, S.K.; Gattmah, J.; Kadhim, H.M. Experimental Investigation of Surface Integrity and Multi-Objective Optimization of End Milling for Hybrid Al7075 Matrix Composites. *Silicon* **2021**, *13*, 1403-1419, https://doi.org/10.1007/s12633-020-00530-1.
29. Arumugam, P.U.; Malshe, A.P.; Batzer, S.A. Dry machining of aluminum–silicon alloy using polished CVD diamond-coated cutting tools inserts. *Surface and Coatings Technology* **2006**, *200*, 3399-3403, https://doi.org/10.1016/j.surfcoat.2005.08.127.
30. Francis Xavier, J.; Ravi, B.; Jayabalakrishnan, D.; Ezilarasan, C.; Jayaseelan, V.; Elias, G. Experimental Study on Surface Roughness and Flank Wear in Turning of Nimonic C263 under Dry Cutting Conditions. *Journal of Nanomaterials* **2021**, *2021*, https://doi.org/10.1155/2021/2054399.

31. Singh, A.; Anandita, S.; Gangopadhyay, S. Microstructural Analysis and Multiresponse Optimization During ECM of Inconel 825 Using Hybrid Approach. *Materials and Manufacturing Processes* **2015**, *30*, 842-851, https://doi.org/10.1080/10426914.2014.973575.
32. Avinash, S.; Balram, Y.; Sridhar Babu, B.; Venkatramana, G. Multi-response optimization of pulse TIG welding process parameters of welds AISI 304 and Monel 400 using grey relational analysis. *Materials Today: Proceedings* **2019**, *19*, 296-301, https://doi.org/10.1016/j.matpr.2019.07.211.
33. Abhang, L.B.; Hameedullah, M. Determination of optimum parameters for multi-performance characteristics in turning by using grey relational analysis. *The International Journal of Advanced Manufacturing Technology* **2012**, *63*, 13-24, https://doi.org/10.1007/s00170-011-3857-6.
34. Sharma, R.C.; Dabra, V.; Singh, G.; Kumar, R.; Singh, R.P.; Sharma, S. Multi-response optimization while machining of stainless steel 316L using intelligent approach of grey theory and grey-TLBO. *World Journal of Engineering* **2022**, *19*, 329-339, https://doi.org/10.1108/WJE-06-2020-0226.
35. Kumar, D.; Mondal, S. Process parameters optimization of AISI M2 steel in EDM using Taguchi based TOPSIS and GRA. *Materials Today: Proceedings* **2020**, *26*, 2477-2484, https://doi.org/10.1016/j.matpr.2020.02.527.
36. Sharma, A.; Yadava, V. Optimization of Cut Quality Characteristics during Nd:YAG Laser Straight Cutting of Ni-Based Superalloy Thin Sheet Using Grey Relational Analysis with Entropy Measurement. *Materials and Manufacturing Processes* **2011**, *26*, 1522-1529, https://doi.org/10.1080/10426914.2011.551910.
37. Mia, M.; Bashir, M.A.; Khan, M.A.; Dhar, N.R. Optimization of MQL flow rate for minimum cutting force and surface roughness in end milling of hardened steel (HRC 40). *The International Journal of Advanced Manufacturing Technology* **2017**, *89*, 675-690, https://doi.org/10.1007/s00170-016-9080-8.
38. Kokubo, T.; Takadama, H. How useful is SBF in predicting in vivo bone bioactivity? *Biomaterials* **2006**, *27*, 2907-2915, https://doi.org/10.1016/j.biomaterials.2006.01.017.
39. Taltavull, C.; Shi, Z.; Torres, B.; Rams, J.; Atrens, A. Influence of the chloride ion concentration on the corrosion of high-purity Mg, ZE41 and AZ91 in buffered Hank's solution. *Journal of Materials Science: Materials in Medicine* **2014**, *25*, 329-345, https://doi.org/10.1007/s10856-013-5087-y.
40. Singh, N.; Batra, U.; Kumar, K.; Mahapatro, A. Investigating TiO2–HA–PCL hybrid coating as an efficient corrosion resistant barrier of ZM21 Mg alloy. *Journal of Magnesium and Alloys* **2021**, *9*, 627-646, https://doi.org/10.1016/j.jma.2020.08.003.
41. Kumar, S.; Saravanan, I.; Patnaik, L. Optimization of surface roughness and material removal rate in milling of AISI 1005 carbon steel using Taguchi approach. *Materials Today: Proceedings* **2020**, *22*, 654-658, https://doi.org/10.1016/j.matpr.2019.09.039.
42. Sukumar, M.S.; Ramaiah, P.V.; Nagarjuna, A. Optimization and Prediction of Parameters in Face Milling of Al-6061 Using Taguchi and ANN Approach. *Procedia Engineering* **2014**, *97*, 365-371, https://doi.org/10.1016/j.proeng.2014.12.260.
43. Saini, M.; Singh, Y.; Arora, P.; Arora, V.; Jain, K. Implant biomaterials: A comprehensive review. *World Journal of Clinical Cases* **2015**, *3*, https://doi.org/10.12998/wjcc.v3.i1.52.
44. Sarkar, S.; Datta, S. Machining Performance of Inconel 718 Under Dry, MQL, and Nanofluid MQL Conditions: Application of Coconut Oil (Base Fluid) and Multi-walled Carbon Nanotubes as Additives. *Arabian Journal for Science and Engineering* **2021**, *46*, 2371-2395, https://doi.org/10.1007/s13369-020-05058-5.
45. Lu, L.; Hu, S.; Liu, L.; Yin, Z. High speed cutting of AZ31 magnesium alloy. *Journal of Magnesium and Alloys* **2016**, *4*, 128-134, https://doi.org/10.1016/j.jma.2016.04.004.
46. Akhtar, W.; Sun, J.; Chen, W. Effect of Machining Parameters on Surface Integrity in High Speed Milling of Super Alloy GH4169/Inconel 718. *Materials and Manufacturing Processes* **2016**, *31*, 620-627, https://doi.org/10.1080/10426914.2014.994769.
47. Dinesh, S.; Senthilkumar, V.; Asokan, P.; Arulkirubakaran, D. Effect of cryogenic cooling on machinability and surface quality of bio-degradable ZK60 Mg alloy. *Materials & Design* **2015**, *87*, 1030-1036, https://doi.org/10.1016/j.matdes.2015.08.099.
48. Kumar, R.; Katyal, P.; Kumar, K.; Sharma, N. Investigating machining characteristics and degradation rate of biodegradable ZM21 magnesium alloy in end milling process. *International Journal of Lightweight Materials and Manufacture* **2022**, *5*, 102-112, https://doi.org/10.1016/j.ijlmm.2021.11.002.
49. Bairagi, D.; Mandal, S. A comprehensive review on biocompatible Mg-based alloys as temporary orthopaedic implants: Current status, challenges, and future prospects. *Journal of Magnesium and Alloys* **2022**, *10*, 627-669, https://doi.org/10.1016/j.jma.2021.09.005.
50. Jangra, K.; Grover, S.; Aggarwal, A. Optimization of multi machining characteristics in WEDM of WC-5.3%Co composite using integrated approach of Taguchi, GRA and entropy method. *Frontiers of Mechanical Engineering* **2012**, *7*, 288-299, https://doi.org/10.1007/s11465-012-0333-4.